Earthquake Engineering, Tenth World Conference © 1992 Balkema, Rotterdam. ISBN 90 5410 060 5

Study on characteristics of near-field seismic motions in a three-dimensional sedimentary basin due to a fault source using Aki and Larner method

H.Uebayashi, Y.Takeuchi & M.Horike
Technical Research Institute, HAZAMA Corporation, Japan

ABSTRACT: In this paper, we have extended the discrete wavenumber method(Aki and Larner method) to make it possible to compute the seismic motion of a three-dimensional(3-D) sedimentary basin with multiple irregular interfaces, due to a seismic fault source. We computed the frequency and time domain response of the 3-D sedimentary basin model resulting from a rectangular dislocation source. Seismic motions of the 3-D sedimentary basin model was then compared with those of the following two models with the corresponding seismic sources: one is a 3-D wavefield with a flat-layer subsurface structure and the other is a 2-D wavefield with an irregular-layer subsurface structure. We also investigated the effects of source parameters on free flat surface responses. From these comparative results, we found that the effects of a seismic source and a 3-D irregular subsurface structure must be taken into account, when predicting strong seismic motion characteristics of nearby shallow earthquakes.

1 INTRODUCTION

Recorded seismograms from the surface strata suggest significant scattering caused by local site conditions (Kudo, Toriumi et al.) and seismic sources(Nat.Res.Cent.Disast.Prev.). Moreover, it has been shown that the path between the source and the local site also influences seismic motion in the surface strata(Yamanaka et al.). Therefore, to predict seismic motion in sedimentary basins we must sum up the effects of the seismic source , the path and the irregular subsurface structure. Since the work of Aki and Larner (1970), many researchers have studied the problem of theoretical seismograms in irregular subsurface structures(Bard et al., Boor, Kawase). Most of these theoretical studies have been carried out within the framework of a two-dimensional(2-D) problem. However, actual seismic sources and subsurface structures are three-dimensional. Few three-dimensional(3-D) subsurface structures and source properties have been considered in the computations of theoretical seismograms(Lee et al., Sanches-Sesma et al., Sato et al.). These methods, however, treat only axisymmetrical subsurface structures. In this paper, we will first extend the Aki and Larner method to make it possible to compute the seismic motion for an arbitrary arrangement of a 3-D subsurface structure and a seismic fault source(Uebayashi et al.,1990,1992, Horike et al.). Then, we will present the numerical results and discuss their features by comparing with the seismic motions in a 3-D wavefield with a flat-layer subsurface structure quantitatively, and in a 2-D wavefield with irregular-layer subsurface structures qualitatively. Moreover, we will investigate the effects of the source parameters such as the dip angle and the location of epicenter on free flat surface responses.

2 METHOD

We decid to calcurate seismic motions in a 3-D sedimentary basin with multiple irregular interfaces, caused by a rectangular dislocation source. The configuration of the problem is shown in Fig.1. Each layer is homogeneous and isotropic.

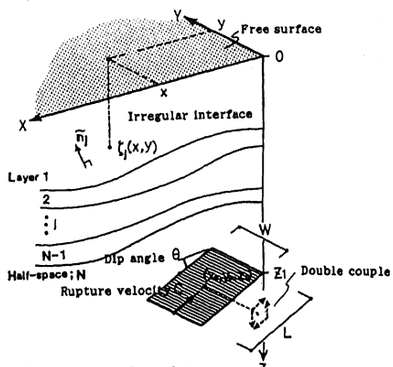

Fig.1 Configuration of problem. Sketch of the three-dimensional multiple irregular interfaces and a rectangular fault source.

Three-dimensional AL method In a 3-D elastic wavefield, the displacement vector can be written in the form(Aki and Richards)

$$u(x,y,z) = grad\varphi + rotrot(0,0,\psi) + rot(0,0,\chi), \quad (1)$$

where φ, ψ and χ, which are referred to as P-, SV- and SH-wave potentials, respectively. They are expressed as

$$\begin{aligned}
\varphi_j(x,y,z) &= \int_{-\infty}^{\infty}\int_{-\infty}^{\infty} \{A_j^+(kx,ky)\cdot\exp(i\nu_j z) + A_j^-(kx,ky)\cdot\exp(-i\nu_j z)\} \\
&\quad \cdot \exp\{i(kx\cdot x + ky\cdot y)\}\,dkx\,dky \\
\psi_j(x,y,z) &= \int_{-\infty}^{\infty}\int_{-\infty}^{\infty} \{B_j^+(kx,ky)\cdot\exp(i\gamma_j z) + B_j^-(kx,ky)\cdot\exp(-i\gamma_j z)\} \\
&\quad \cdot \exp\{i(kx\cdot x + ky\cdot y)\}\,dkx\,dky \\
\chi_j(x,y,z) &= \int_{-\infty}^{\infty}\int_{-\infty}^{\infty} \{C_j^+(kx,ky)\cdot\exp(i\gamma_j z) + C_j^-(kx,ky)\cdot\exp(-i\gamma_j z)\} \\
&\quad \cdot \exp\{i(kx\cdot x + ky\cdot y)\}\,dkx\,dky
\end{aligned} \quad (2)$$

in the j-th layer($j \neq N$), where the time factor $e^{-i\omega t}$ is omitted and kx and ky are horizontal wavenumbers. Vertical wavenumbers ν_j, γ_j are defined as $\nu_j=(\omega^2/\alpha_j^2-kx^2-ky^2)^{1/2}$ and $\gamma_j=(\omega^2/\beta_j^2-kx^2-ky^2)^{1/2}$, respectively, where α_j and β_j denote the compressional and the shear velocities. Assuming the Rayleigh ansatz(Aki et al.), on the other hand, the displacement potentials in a half-space are expressed as

$$\begin{aligned}
\varphi_N(x,y,z) &= \varphi_0(x,y,z) + \int_{-\infty}^{\infty}\int_{-\infty}^{\infty} A_N^-(kx,ky) \\
&\quad \cdot \exp\{i(kx\cdot x + ky\cdot y + \nu_N\cdot z)\}\,dkx\,dky \\
\psi_N(x,y,z) &= \psi_0(x,y,z) + \int_{-\infty}^{\infty}\int_{-\infty}^{\infty} B_N^-(kx,ky) \\
&\quad \cdot \exp\{i(kx\cdot x + ky\cdot y + \gamma_N\cdot z)\}\,dkx\,dky \\
\chi_N(x,y,z) &= \chi_0(x,y,z) + \int_{-\infty}^{\infty}\int_{-\infty}^{\infty} C_N^-(kx,ky) \\
&\quad \cdot \exp\{i(kx\cdot x + ky\cdot y + \gamma_N\cdot z)\}\,dkx\,dky\ ,
\end{aligned} \quad (3)$$

where φ_0, ψ_0 and χ_0 are source potentials and are introduced in the latter half of this chapter. ν_N and γ_N are defined as $\nu_N=(\omega^2/\alpha_N^2-kx^2-ky^2)^{1/2};Im(\nu_N)>0$ and $\gamma_N=(\omega^2/\beta_N^2-kx^2-ky^2)^{1/2};Im(\gamma_N)>0$.

Assuming spatial periodicity of a wavefield with intervals Lx and Ly in the two horizontal directions, Eqs.(2) and (3) can be approximately replaced by finite sum over the two discrete wavenumbers ${}_lkx$, ${}_nky$ which are defined as ${}_lkx=2\pi l/Lx$ and ${}_nky=2\pi n/Ly$ where $l=0,\pm1,\pm2,\cdots,\pm Nx$ $n=0,\pm1,\pm2,\cdots,\pm Ny$ where Nx and Ny are the truncation numbers of two horizontal wavenumbers.

Using matrix notation, displacement and traction components on the j-th layer side of the interface are represented in the form

$$\begin{Bmatrix} u_x(x,y) \\ u_y(x,y) \\ u_z(x,y) \\ \tau\bar{n}_x(x,y) \\ \tau\bar{n}_y(x,y) \\ \tau\bar{n}_z(x,y) \end{Bmatrix}_j = -\sum_{l=-Nx}^{Nx}\sum_{n=-Ny}^{Ny} [\,L(l,n,x,y)\,]_{(j)(x,y)}\cdot e(l,n,x,y) \begin{Bmatrix} A^+(l,n) \\ B^+(l,n) \\ C^+(l,n) \\ A^-(l,n) \\ B^-(l,n) \\ C^-(l,n) \end{Bmatrix}_j \quad (4)$$

where $e(l,n,x,y)=\exp[2\pi i(lx/Lx+ny/Ly)]$ and $[L]$ is the 6×6 matrix. Similarly, components on the half-space side are represented in the form

$$\begin{Bmatrix} u_x(x,y) \\ u_y(x,y) \\ u_z(x,y) \\ \tau\bar{n}_x(x,y) \\ \tau\bar{n}_y(x,y) \\ \tau\bar{n}_z(x,y) \end{Bmatrix}_N = -\sum_{l=-Nx}^{Nx}\sum_{n=-Ny}^{Ny} [\,H(l,n,x,y)\,]_{(N-1)(x,y)}\cdot e(l,n,x,y) \begin{Bmatrix} A^+(l,n) \\ B^+(l,n) \\ C^+(l,n) \end{Bmatrix}_N + [\,H'(l,n,x,y)\,]_{(N-1)(x,y)}\cdot e(l,n,x,y) \begin{Bmatrix} A_0(l,n) \\ B_0(l,n) \\ C_0(l,n) \end{Bmatrix} \quad (5)$$

where $[H]$ and $[H']$ are the 6×3 matrices.

From the stress free condition in the first layer at the surface, the coefficients $A^-(l,n)$, $B^-(l,n)$ and $C^-(l,n)$ can be expressed by the coefficients $A^+(l,n)$, $B^+(l,n)$ and $C^+(l,n)$.

$$\begin{Bmatrix} A^-(l,n) \\ B^-(l,n) \\ C^-(l,n) \end{Bmatrix}_1 = [\,F\,] \begin{Bmatrix} A^+(l,n) \\ B^+(l,n) \\ C^+(l,n) \end{Bmatrix}_1 \quad (6)$$

where $[F]$ is 3×3 matrix. From the conditions of the continuity of displacements and stresses at the interface between the j-th and the (j-1)-th layers, we obtain follows:

$$[\,G\,]_B^{j-1}\{A\}^{j-1} = [\,G\,]_A^j\{A\}^j \quad (1<j<N) \quad (7)$$

where matrices $[G]_B^{j-1}$ and $[G]_A^j$ are defined at the deeper interface of the (j-1)-th layer and at the shallower interface of the j-th layer, respectively, and $\{A\}^j=\{A^+(l,n),B^+(l,n),C^+(l,n),A^-(l,n),B^-(l,n),C^-(l,n)\}_j^T$. Similarly, applying the boundary conditions between half-space(N-th layer) and (N-1)-th layer, we obtain

$$[\,G\,]_B^{N-1}\{A\}^{N-1} = [\,G_1\,]^N\{A\}^N + [\,G_2\,]^N\{A_0\} \quad (8)$$

where $[G_1]^N$, $[G_2]^N$ are 6×3 matrces for half-space, $\{A\}^N=\{A^+(l,n),B^+(l,n),C^+(l,n)\}_N^T$, $\{A_0\}=\{A_0(l,n),B_0(l,n),C_0(l,n)\}^T$. The following equation from Eqs.(7) and (8): is obtained:

$$[\,D\,]\{A\}^1 = [\,G_1\,]^N\{A\}^N + [\,G_2\,]^N\{A_0\} \quad (9)$$

where $[D]=[G]_B^{N-1}[E]$, $[E]=[R]^{N-1}[R]^{N-2}\cdots[R]^2$ and $[R]^j=[G]_B^{j-1}[G]_A^j$. We rearrange Eq.(9) by substituting Eq.(6) into Eq.(9).

$$[\,M\,]\{A\} = [\,G_2\,]^N\{A_0\} \quad (10)$$

where $\{A\}=\{A_1^+(l,n),B_1^+(l,n),C_1^+(l,n),A_N^-(l,n),B_N^-(l,n),C_N^-(l,n)\}^T$.

Taking the spatial Fourier transform of the matrix elements of Eq.(10) by integrating over $0<x<Lx$ and $0<y<Ly$, the $6(2Nx+1)(2Ny+1)$ simultaneous linear equation for the vector$\{A\}$ is obtained. Using the vector $\{A^+(l,n),B^+(l,n),C^+(l,n)\}_1^T$ obtained from solving Eq.(10), we obtain the vector$\{A^-(l,n),B^-(l,n),C^-(l,n)\}_1^T$(Eq.(6)) Finally, substituting the vector$\{A\}$ in the first layer for Eq.(4), free surface responses in the frequency domain are obtained.

Source potential Using the potentials caused by elementary point forces presented by Bouchon(1979), we can be obtained the source potentials of dip slip faults with any dip angle. We treat the following equations different form Eqs.(1) and (2):

$$\begin{aligned}
&u(x,y,z) = grad\,\varphi + rot\,\psi, \\
&div\,\psi = 0\ ,\ \psi=(\psi_1,\psi_2,\psi_3),
\end{aligned} \quad (11)$$

$$\begin{aligned}
\varphi(x,y,z) &= \int_{-\infty}^{\infty}\int_{-\infty}^{\infty} a(kx,ky)\cdot\exp\{i(kx\cdot x + ky\cdot y - \nu_N\cdot z)\}\,dkx\,dky \\
\psi_j(x,y,z) &\cdot \int_{-\infty}^{\infty}\int_{-\infty}^{\infty} b_j(kx,ky)\cdot\exp\{i(kx\cdot x + ky\cdot y - \gamma_N\cdot z)\}\,dkx\,dky
\end{aligned} \quad (12)$$

Applying the force-dislocation equivalence(Burridge et al.) for a fault source, the coefficients a and b_j (j=1,2,3) are obtained as

$$\begin{aligned}
a(l,n) &= \frac{\mu_N\cdot D}{F}\int_s \{(\frac{\partial\varphi^x}{\partial x}+\frac{\partial\varphi^z}{\partial z})\cdot(\sin^2\theta-\cos^2\theta)+2(\frac{\partial\varphi^x}{\partial x}-\frac{\partial\varphi^z}{\partial z}) \\
&\quad \cdot \sin\theta\cdot\cos\theta\}\cdot\exp(-\frac{i\omega}{C\cdot\cos\theta}x_0) \\
&\quad \cdot \exp\{-i({}_lkx\cdot x_0 + {}_nky\cdot y_0 - {}_{l,n}\nu_N\cdot z_0)\}\,ds \\
b_j(l,n) &= \frac{\mu_N\cdot D}{F}\int_s \{(\frac{\partial\psi_j^x}{\partial x}+\frac{\partial\psi_j^z}{\partial z})\cdot(\sin^2\theta-\cos^2\theta)+2(\frac{\partial\psi_j^x}{\partial x}-\frac{\partial\psi_j^z}{\partial z}) \\
&\quad \cdot \sin\theta\cdot\cos\theta\}\cdot\exp(-\frac{i\omega}{C\cdot\cos\theta}x_0) \\
&\quad \cdot \exp\{-i({}_lkx\cdot x_0 + {}_nky\cdot y_0 - {}_{l,n}\gamma_N\cdot z_0)\}\,ds
\end{aligned} \quad (13)$$

where C is the rupture velocity. μ_N is the shear rigidity of the half-space medium, θ is the dip angle, and S is the area of the

rupture zone. F is the concentrated force. (x_0, y_0, z_0) is a local coordinate on the fault plane with an origin located at $(x,y,z)=(0,0,z_1)$. Then, $(\bar{x},\bar{y},\bar{z})$ are $\bar{x}=x-x_0$, $\bar{y}=y-y_0$, $\bar{z}=z-z_0$. The displacement potentials φ^x, φ^z, ψ_j^y and ψ_j^z result from a point force applied at the origin of coordinate $(\bar{x},\bar{y},\bar{z})$, where suffix j is x-, y-, z-components, respectively. Finally, the coefficients A_0, B_0 and C_0 from the Eq.(10), can be obtained from the following equations.

$$
\begin{aligned}
&A_0(l,n)=a(l,n)\\
&B_0(l,n)=i/(\mu k x^2+\rho k y^2)\cdot\{\mu k x\cdot b_2(l,n)-\rho k y\cdot b_1(l,n)\}\\
&C_0(l,n)=b_3(l,n)+\gamma_N/(\mu k x^2+\rho k y^2)\cdot\{\mu k x\cdot b_1(l,n)+\rho k y\cdot b_2(l,n)\}
\end{aligned}
\qquad (14)
$$

3 NUMERICAL EXAMPLES

We use the 3-D sedimentary basin model with a irregular interface shown in Fig.2. The geophysical constants of these subsurface structural models are shown in Table 1, but damping is not included in these media.

Accuracy In a sedimentary layer of the trapezoidal model, the phase velocity of the fundamental mode of the Rayleigh waves is larger than the S-wave velocity of the sedimentary layer in the computed frequency range between 0 and 0.60Hz (Fig.3). This mean that the truncation numbers Nx and Ny depend on the S-wave velocity in the sedimentary layer.

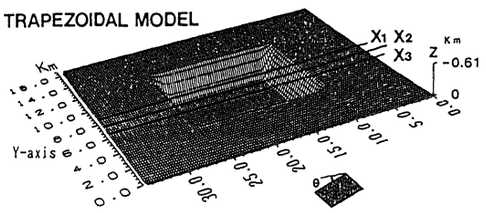

Fig.2 Configuration of a irregular interface and a fault source. A few parameters are fixed as follows; focal depth is 4.5km, fault length and width are 2.4km and 1.2km, respectively, rupture velocity is 1.2km/s.

Table 1 Geophysical constants

	Layer	Half-space
P-wave velocity(km/s)	2.0	4.0
S-wave velocity(km/s)	0.7	2.0
Density(g/cm^3)	1.8	2.5

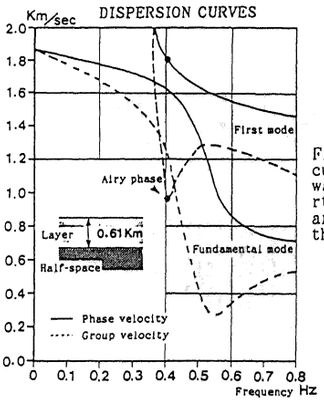

Fig.3 Dispersion curves of Rayleigh waves. Soil properties of each layer are the same as those in table 1.

We check the accuracy of the free surface responses indirectly from the convergence of the coefficients for SV and SHwave potentials at frequency 0.28Hz on a free surface. This frequency is nearly equal to the fundamental predominant frequency($\beta_1/4H$). As shown in Fig.4, the maximum value of the coefficient in the truncation number(Nx=±14, Ny=±7) is -15.7db(approximately 1/25) in the SV wave potentials. This means that the coefficients for each wave potential at 0.28Hz almost converge. Therefore, we evaluate that the free surface responses are not heavily contaminated by the truncation of wavenumbers

The source time functions are shown in Fig. 5. The duration time is 100s. Therefore, the fundamental frequency Δf is 0.01Hz. In the frequency responses, we calculated strictly for 31 frequencies with an interval of 0.02Hz between 0 and 0.60Hz, and the frequency responses at the intermediate frequencies are approximately interpolated. To examine the accuracy of the frequency responses obtained by this procedure, we compare the seismic motions at two frequency responses(Fig.6) : one response is interpolated by the above procedure and the other is strictly computed over the entire frequency range. Figure 6 shows the close matching of the two seismic motions in the sedimentary basin.

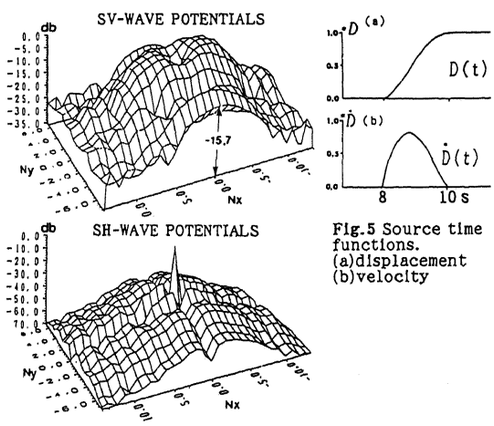

Fig.5 Source time functions.
(a)displacement
(b)velocity

Fig.4 Amplitude distributions of displacement potentials in the wavenumber domain at the free surface resulting from a fault source with a dip angle of $\pi/4$. The epicenter locates at the center of the basin.

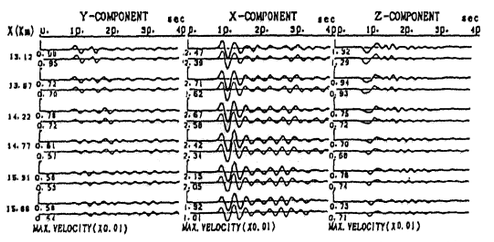

Fig.6 Comparison of seismic motions at sites on line X_2, between the frequency responses interpolated (bold lines) and strictly(fine lines).

In this paper, since the effect of the scattered waves caused by adjacent sources (Bouchon) may be much larger than effects caused by adjacent irregular interfaces, we investigate about the effect of adjacent sources(Figs.7 and 8). In the time window (0 to 40s) of the seismic motions shown in the later section, the intervals Lx and Ly of source must be larger than 160km($40s \times \alpha_2$) to except the effects of the scattered waves coming from adjacent sources. However, since the computation of the 3-D wavefield with such long intervals takes up a vast capacity of the main memory of the computer, we estimate the error of the seismic motions computed with the intervals Lx=35km and Ly =17.5km ,indirectly.

Seismic motions on the free surface of the trapezoidal model due to a vertical dip slip fault with intervals Lx=35km and Ly=17.5km are compared with those obtained from the following two steps(Fig.8): one is to compute the seismic motion Vi at a site(x=17.5,y=8.75,z=0.61km) in a infinite medium due to the same source as above, but with intervals of 160km (Fig.7(a)), the other is to compute the seismic motions Vp on the free surface of the trapezoidal model due to a vertical incidence of a plane S-wave with the motion Vi obtained from the previous step. Therefore, the motion Vp are not a results of the scattered waves coming from adjacent sources. As shown in Fig.8, the main phases in the two motions Vs and Vp at sites in the basin center correspond to each other. This means that the error caused by adjacent sources is some effect.

Frequency response characteristics Figure 9 shows the amplitude distributions of surface displacement spectra in the trapezoidal model at the frequencies 0.1, 0.3 and 0.45Hz, due to the fault source located under the basin centers and the basin edges. Comparing the distribution shapes between the upper and the lower diagrams at the frequency of 0.1Hz, these shapes are resemblance each other, irrespective of epicenter locations. However, in proportion as the frequencies increase, these shapes become quite different. This means that the seismic responses of the ground surface are principally influenced by source parameters such as the dip angle in the lower frequency range, and in the higher frequency being influenced by the 3-D subsurface structure in addition to source parameters.

Comparison of seismic motions between the 3-D sedimentary basin and the flat layered subsurface structure To examine the features of the seismic motions of a 3-D sedimentary basin caused by a fault source, we compare the seismic motions between the trapezoidal and the flat-layer models at sites on the lines X_1,X_2 and X_3(Fig.10). The vertical dip slip fault is located just under the basin edges(X=11.0km,Y=8.75km). In the sedimentary basin, the maximum amplitudes (shown beneath each time axis and a unit is $10^{-2} \times$ D/s) of the trapezoidal model are, at most sites, larger than those of the flat-layer model. Moreover, the feature of the waveforms(except for the onset portions) in the trapezoidal model shows that the phase(Rp) propagating in the direction of positive X, can be clearly

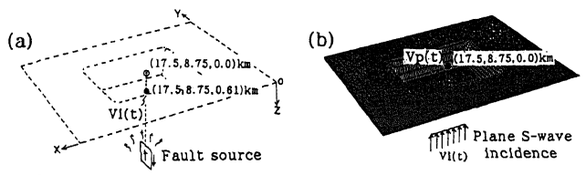

Fig.7 Configuration for examination of the error caused by adjacent sources. (a)Sketch of an infinite medium and a vertical dip slip fault. Geological constants are the same as those of the half-space in Table1. (b)Sketch of the trapezoidal model and a plane S-wave incidence. Seismic motions Vp at the free surface caused by the input motion VI are obtained.

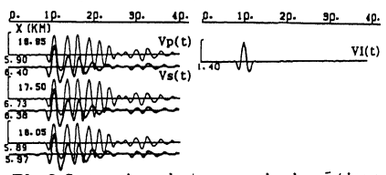

Fig.8 Comparison between seismic motions Vs and Vp(see Fig.7). Vs is the seismic motion on the free surface of the trapezoidal model due to a vertical dip slip fault with intervals Lx=35km, Ly=17.5km.

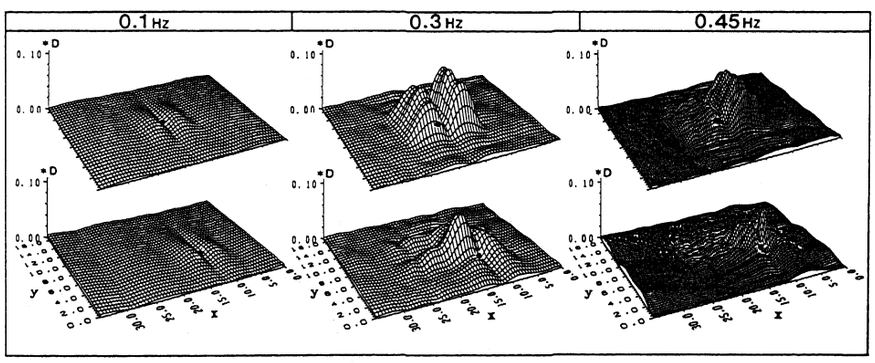

Fig.9 Amplitude distributions of surface displacement spectra by the same parameters as Fig.4. The black dots denote the location of the epicenter.

seen at all lines. The velocity of the phase (Rp) is approximately 1.8km/s. To examine the features of this phase, the frequency responses in the trapezoidal model at the site(X=16.41km,Y=8.75km) are indicated in Fig.11. The predominant frequency is approximately 0.40Hz. In Fig.3, those peaks correspond to the Airy phase of the first mode of the Rayleigh waves. Moreover, the phase velocity (approximately 1.8km/s) corresponding to this Airy phase is nearly equal to that of the phase(Rp) mentioned above. This means that the Rp-phase waves are mainly Rayleigh waves of the first mode, which are generated at the basin edges.

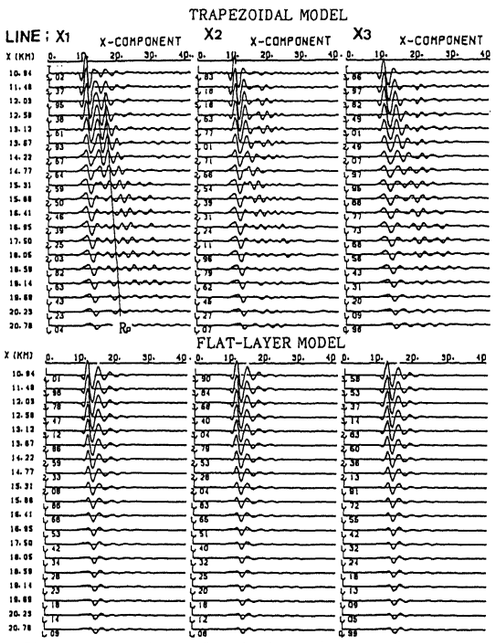

Fig.10 Comparison of seismic motions at sites on lines X_1,X_2 and X_3 in the trapezoidal and the flat layered models due to a vertical dip slip fault located under the basin edges(X=11.0km,Y=8.75km).

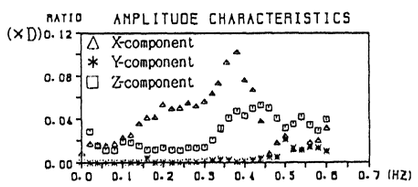

Fig.11 Frequency response spectra at the site (X=16.41km,Y=8.75km) in the trapezoidal model corresponding to Fig.10.

Comparison of seismic motions between the 3-D and 2-D wavefields with irregular-layer subsurface structure The 2-D sedimentary basin model is the same as the cross section beneath line X_1 in the 3-D sedimentary basin model(Fig. 2).

Figure 12 shows the seismic motions of the 2-D model and is compared with those of the 3-D model shown in Fig.10. Seismic motions of the 2-D model, however, cannot be directly compared with those of the 3-D model, because of the differences in the source properties for example, the seismic moment. Therefore, we examine the qualitative feature such as the waveforms and the spatial variations. During the propagation of the phase(Rp) in the direction of positive X, the amplitude of the phases of the 3-D model decreases rapidly, while that of the 2-D model changes little. In contrast, the amplitude of onset portions in the 3-D model due to direct S-waves is larger at the near sites (X<16.41km) and smaller at the far sites(18.05km<X) of the epicenter than those of the 2-D model. These comparative results mean that the 3-D seismic motions cannot be replaced by the 2-D seismic motions.

Next we will investigate the effects of the dip angle on seismic motions. Figs.13 and 14 show the comparisons between the 3-D and 2-D seismic motions due to the thrust fault with a dip angle of zero-degrees and the dip slip

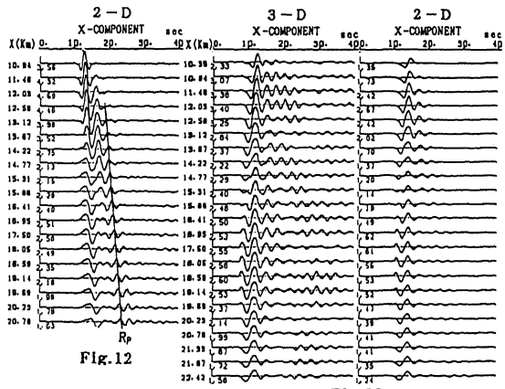

Fig.12

Fig.13

Fig.12 Seismic motions of the 2-D wavefield with an irregular interface due to a 2-D vertical dip slip fault located under the basin edges.

Fig.13 Comparison of seismic motions, between the 3-D and the 2-D wavefields with an irregular interface due to a thrust fault with a dip of zero-degrees. Epicenter locates at the center of the basin.

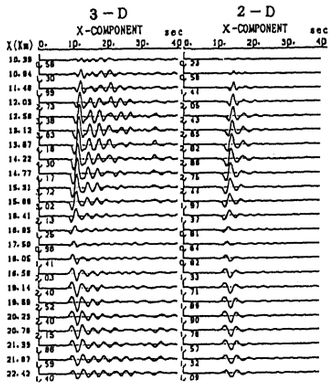

Fig.14 The same as Fig.13, but for a dip angle of $\pi/4$.

fault with a dip angle of $\pi/4$, respectively. As shown in Figs. 13 and 14, the sites of the 3-D model with long duration seismic motions are in the middle of the basin for the thrust fault, and around the circumference of the basin for the dip angle $\pi/4$. However, in spite of the dip angle, the duration of the seismic motion in the 2-D model change little spatially. These features mean that the seismic motions of the 3-D model vary more according to the dip angle when compared to those of the 2-D model.

4 DISCUSSION AND CONCLUSION

The surface displacement spectra in the 3-D sedimentary basin model due to a dislocation source show that the amplitude characteristics are principally influenced by source parameters in the range of lower frequency, and are influenced by the 3-D subsurface structure in addition to the source parameters in the range of higher frequency.

Comparing seismic motions of the 3-D sedimentary basin and the flat-layer models due to a rectangular dislocation source, the seismic motions of the 3-D sedimentary basin model are much greater in spatial variation (except for the onset portions), larger in maximum amplitude, and much longer in duration than those of the flat-layer model.

Comparing seismic motions in the 3-D and 2-D wavefields with an irregular subsurface structure due to the source corresponding to respective wavefields, seismic motions in the 3-D wavefield are greater in spatial variation (except for the onset portions) than those in the 2-D wavefield at all sites in the basin. Moreover, the seismic motions in the 3-D wavefield vary more according to the source parameters, than those in the 2-D wavefield.

These differences in seismic motions between the 3-D sedimentary basin and the other models are mainly caused by the local surface waves generated at the periphery of the basin. Generation of local surface waves strongly depend upon the location of the epicenter and the seismic wave radiation pattern. In particular, when the following conditions are satisfied, the local surface waves are generated most effectively: The seismic fault is located beneath the basin sides. S-wave radiation caused by the double couple hit the basin sides.

We have arrived at the following conclusion. When predicting seismic ground motions in a near-field, the effects of the seismic source and the 3-D irregular subsurface structures must be taken into account.

The computations were carried out mainly on a FACOM VP-400E (1.7GFLOPS,main storage;256MB) of the Data Processing Center of Kyoto University. Summary of the system messages of the job (truncation numbers;Nx=10,Ny=19, sampling points;64x128, a frequency response at 0.4Hz) executed by this computer are follows:

CPU time:1395.46s*(including the vector unit time;1223.82s)
Region size : approximately 185MB
The vectorized ratio : 98.9%

*) half as long again as that in the case of plane wave incidence

REFERENCES

Aki,K. and K.L. Larner, Surface motion of layered medium having an irregular interface due to incident plane SH waves., J. Geophys. R., Vol. 75, 933-954, 1970.

Aki,K. and P. G. Richards, Quantitative seismology Theory and Methods Vol.1, 2 W.H.Freeman and company New york., 215-216, 807-812, 1980.

Bard,P.Y. and M. Bouchon, The seismic response of sediment-filled valleys Partl and 2., Bull. Seism. Soc. Am., Vol.70, 1921-1941, 1263-1286,1980a,b.

Boor,D.M.,Finite difference methods for seismic propagation in heterogeneous materials., Methods in Computation Physics, Vol.12, 1-31,1972.

Bouchon,M. Discrete wave number representation of elastic wave fields in three-dimensions., J. Geophys. R., Vol.84, 3609-3614, 1979.

Burridge,R and L. Knopoff, Body force equivalents for seismic dislocations, Bull. Seism. Soc. Am., Vol.54, 1875-1888, 1964.

Horike,M., Uebayashi,H. and Takeuchi,Y. Seismic response in three-dimensional sedimentary basin due to plane S wave incidence., J. Phys. Earth., Vol.33, 261-284, 1990.

Kawase,H. Time-domain response of a semicircular canyon for incident SV, P, and Rayleigh waves calculated by the discrete wavenumber boundary element method., Bull. Seismol. Soc. Am., Vol.78, 1415-1437, 1988.

Kudo,K. The study on the contribution of surface waves to strong ground motions., Proc.7th W.C.E.E., 499-506, 1980.

Lee,J.J. and Lagston,C.A. Wave propagation in a three-dimensional circular basin., Bull. Seism. Soc. Am., Vol.73, 1637-1653, 1983.

Sanches-Sesma,F.J., L.E. Perez-Rocha, and S. Chavez-Perez, Diffraction of elastic waves by three-dimensional surface irregularities., Bull.Seism.Soc.Am., Vol.73, 1621-1636, 1989.

Sato,T., Hasegawa,M., Nakai,S., Watanabe,T., and Tanaka,T., Analysis of theoretical seismograms by the thin layer finite element method and its application to the 1980 IZU-HANTO-TOHO-OKI earthquake in Japan, Proc.9th W.C.E.E., Vol.2, 763-768, 1988

The National Research Center for Disaster Prevention, The survey of earthquake damages in vicinity of seismic faults., Research notes the national research center for disaster prevention., 1979

Toriumi,I., Ohba,S. and Murai,N. Earthquake motion characteristics of Osaka plain., Proc.8th W.C.E.E., 761-768, 1984

Uebayashi,H., Horike,M. and Takeuchi,Y., Seismic motion in a three-dimensional arbitrarily-shaped sedimentary basin, due to a rectangular dislocation source., J. Phys. Earth., Vol.40, 223-240, 1992.

Uebayashi,H., Horike,M. and Takeuchi,Y., Seismic responses of a three-dimensional sedimentary basin with an irregular interface to a rectangular dislocation source in a half-space., Journal of Struct. Constr. Engng, AIJ.,NO.413, 75-86, 1990(in Japanese)

Yamanaka,H., Seo,K. and Samano,T. Effects of sedimentary layers on surface wave propagation., Bull.Seismol.Soc.Am., Vol.79, 631-644, 1989